

	001
	002
	003
	004
	005
	006
	007
Brain Dynamics	008
	009
	010
	011
Alexander Mark Weber ^{1,2*}	012
	013
	014
¹ BC Children's Hospital Research Institute, The University of British Columbia, 938 West 28th Avenue, Vancouver, V5Z 4H4, Canada.	015
	016
	017
² Pediatrics, The University of British Columbia, 2329 West Mall, Vancouver, V6T 1Z4, Canada.	018
	019
	020
	021
	022
Corresponding author(s). E-mail(s): aweber@bcchr.ca ;	023
	024
	025
	026
Abstract	027
An introduction to the idea of brain dynamics in fMRI studies	028
	029
	030
	031
	032
¹ The University of British Columbia	033
	034
² The University of British Columbia	035
	036
* Correspondence: Alexander Mark Weber < aweber@bcchr.ca >	037
	038
	039
	040
	041
	042
Introduction	043
Like many physiological data, neurological signals — such as fMRI-BOLD — appear as irregular time-series. Often thought of as being random or noisy, there was an initial	044
	045
	046

047 tendency to measure them statistically, such as calculating their standard deviation,
048 assuming that the elements of the series were independent. However, this approach
049 is inadequate when events exhibit interdependence, whether through short- or long-
050 range temporal correlations (LRTCs) [1]. Therefore, there is a need for methods that
051 can both identify and characterize random noise from irregular but structured and
052 correlated noise. One such method used for LRTCs is the fractal method.
053

054
055
056
057 A fractal structure, either spatial or temporal, is composed of smaller parts that
058 exhibit the same pattern at every scale [2–4]. Classic spatial examples of fractals
059 in nature are coastlines [4], circulatory system [5], and brain anatomy [6], where at
060 each level of magnification these structures look the same; i.e. *self-similarity*. For
061 a dynamic process, or in the temporal domain, this is known as *scale invariance*,
062 meaning that both rapid and slow processes follow the same pattern [7]. These scale-
063 free LRTCs exhibit a gradual decay in their autocorrelation function, indicating that
064 the system maintains a long-lasting, multiscale memory of its past states, which play a
065 role in shaping its present behaviour. Scale-free behavior is a signature characteristic
066 of complex systems that can be understood as the collective outcome of numerous
067 interacting components with weak and random connections [8]. Physiological systems,
068 such as the brain, require a mix of randomness and structure to function optimally
069 [9]. In many cases, this balance between order and randomness allows the system to
070 remain adaptable and responsive to changing conditions [10, 11]. This adaptability is
071 particularly evident when a system is operating near what is called a ‘critical point’,
072 the phase change between order and disorder. When a system is operating near the
073 critical point, it is expected to exhibit LRTCs. Therefore, by analyzing the LRTC of
074 a time-series, valuable insights can be found into the underlying mechanisms driving
075 system behavior, such as memory effects, self-organization, and criticality [12].
076
077
078
079
080
081
082
083
084
085
086
087
088
089
090
091
092

“Because pink noise lies between white and Brown(ian) noise, it has been proven to bring stability and adaptability into dynamic processes, thus, crucial properties of well-functioning complex systems” [9]	093
	094
	095
	096
	097
	098
	099
“as pink noise arises from the interaction of multiple systems and operates over different scales, it has been shown to contribute to system resiliency and structural integrity if individual components were lost or interrupted” [10, 11]	100
	101
	102
	103
	104
See Herman et al. [13] for a really good review	105
	106
Another good review is by Werner (2010) linking fractals/Hurst and Criticality Werner [14]	107
	108
	109
	110
	111
	112
	113
	114
	115
	116
	117
	118
	119
	120
	121
	122
	123
	124
	125
	126
	127
	128
	129
	130
	131
	132
	133
	134
	135
	136
	137
	138

139 Fractal Dimension and Hurst Exponent

140

141 Non-periodic fluctuations are prevalent in physiological systems, and these irregular
142 patterns can be mathematically modeled using stochastic, chaotic, or noisy chaotic
143 methods. Stochastic models assume that the fluctuations result from a large number
144 of weak influences, while chaotic models conceptualize that strong nonlinear inter-
145 actions between a few factors shape the fluctuations. Among the various stochastic
146 approaches, ‘fractal’ models offer the most accurate representation of reality by con-
147 sidering the self-similar nature of physiological fluctuations over different time scales
148 [17]. Fractal structures were first expressed in the late 19th and early 20th century by
149 mathematicians who generated complex geometrical structures with simple objects
150 (e.g. a triangle) by applying a simple rule of transformation in an infinite number
151 of iterative steps Figure 1. A use-case for these geometric structures was not fully
152 realized until the 1960s, when Benoit Mandelbrot formalized them as a new form of
153 geometry capable of describing the complex shapes and forms of nature [4].
154

155

156

157

158

159

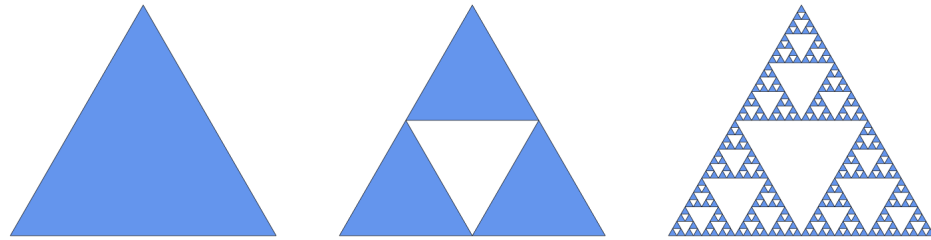
160

161

162

163

164



165

166

167

168

169

170

171

172

173 **Figure 1. Ideal mathematical fractal.** The 2D Sierpinski triangle starts with a
174 simple equilateral triangle (left), and subdivides it recursively into smaller equilateral
175 triangles. For every iteration, each triangle (in blue) is further subdivided it into four
176 smaller congruent equilateral triangles with the central triangle removed. The first
177 such iteration is shown in the centre, with the fifth iteration shown on the right.
178

179

180

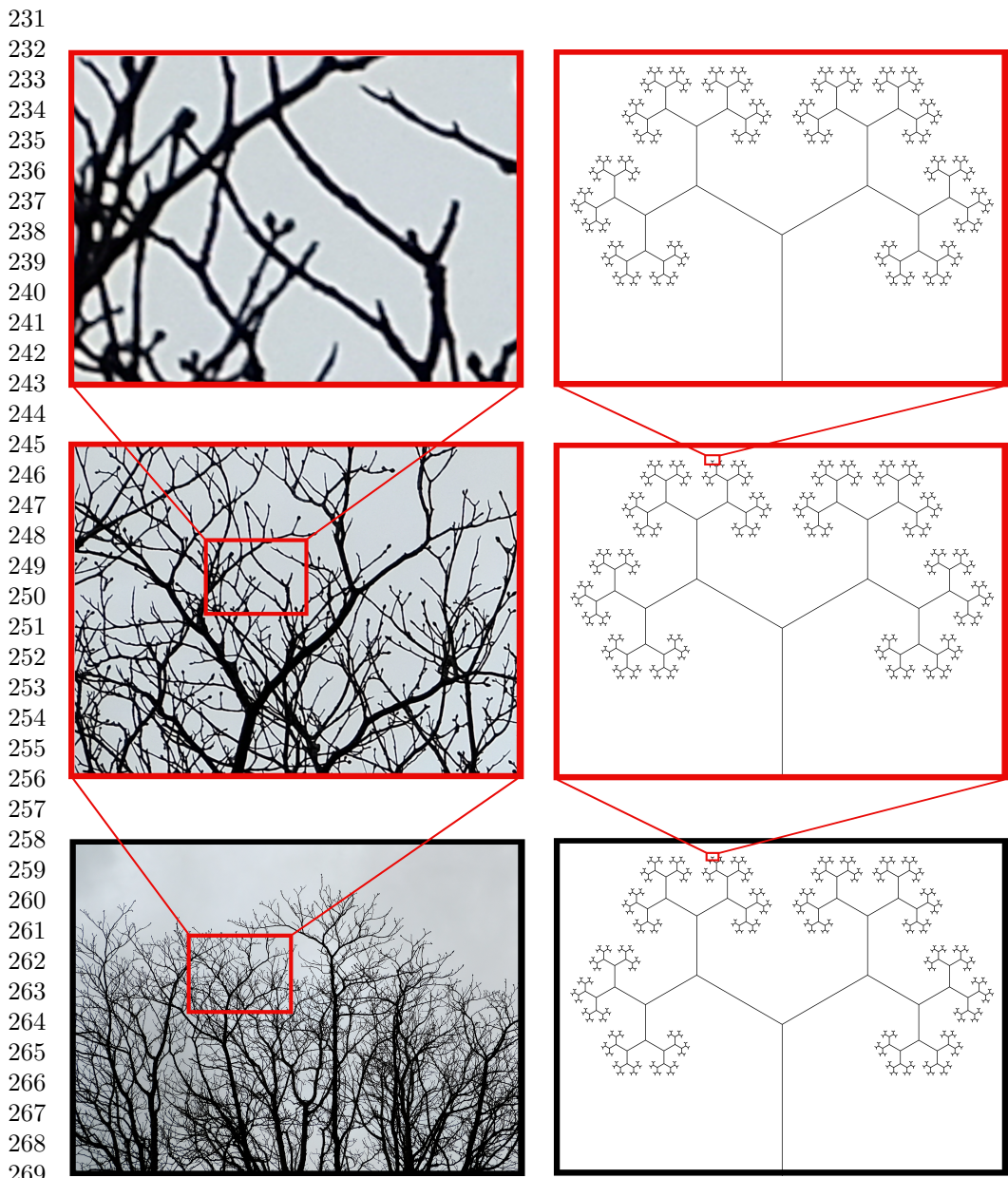
181

182

183

184

Unlike Euclidean structures that can use axioms and rules to describe an object of integer dimensions, fractal structures can only be characterized by recursive algorithms that extend the use of dimension to the non-integer range [18]. Recognizing this difference, Mandelbrot named these complex structures ‘fractals’, and defined their non-Euclidean dimension as a ‘fractal dimension’ (FD) — that is, a non-integer. For the one-dimensional time-series, FD will be between 1 and 2. While a structure such as the Sierpinski triangle is an ‘exact fractal’, meaning it is assembled from pieces that are an exact replica of the whole, nature is composed of ‘statistical fractals’, whose self-similarity is found in the power law scaling of the parameters characterizing their structures at different scales of observation Figure 2. Unlike Euclidean structures which can be defined by axioms, fractals can only be characterized by a set of properties that, when present, indicate the structure is indeed fractal (see Section 2).	185 186 187 188 189 190 191 192 193 194 195 196 197 198 199 200 201 202 203 204 205 206 207 208 209 210 211 212 213 214 215 216 217 218 219 220 221 222 223 224 225 226 227 228 229 230
The Hurst exponent (H) is a statistical measure used to quantify long-range dependence or persistence in time-series data (i.e. LRTCs). First introduced by Harold Hurst in 1951 for hydrological applications [20], it was Mandelbrot again who helped popularize its use for studying complex shapes and forms of nature [4, 21]. Since then it has been applied across various fields, including finance, geophysics, ecology, and neuroscience, to characterize complex systems with intricate dynamics [22–25]. H and FD for time-series can be directly converted, as	219 220 221 222 223 224 225 226 227 228 229 230
$H = 2 - D.$	(1)
This means that FD and H are inversely correlated, and that H is a real number between 0 and 1 (non-inclusive; although it can be extended to > 1 ; see ...). For the rest of this paper, we will be discussing H .	221 222 223 224 225 226 227 228 229 230



270 **Figure 2. A comparison of statistical and exact fractal patterns.** The two
 271 basic forms of fractals are demonstrated. Zooming in on tree branches (left), an exact
 272 self-similar element cannot be found. Zooming in on an exact fractal (right), exact
 273 replica of the whole are found. Photo by author. Branching fractal made in Python.
 274 Figure inspired by Taylor (2006) [19]

275
 276

Thus, the basic premise behind fractal time-series analysis is: beneath the seemingly chaotic and unpredictable variations in the signal, there lies a stable underlying mechanism which can be effectively described using only a few possible parameters (i.e. H or FD).

Properties

When $H = 0.5$ ($FD = 1.5$), the time-series is completely uncorrelated, has no memory, and is like white noise (pure random). It represents the highest level of unpredictability and entropy, but not necessarily the most complex state in a physiological sense. When $H < 0.5$ ($FD > 1.5$), the time-series is said to be anti-persistent, exhibiting negative correlations: i.e. if the signal increases at one point, it's likely to decrease at the next point. This is also known as short-term reversal. This tends to make the time-series more predictable and reduces randomness, often simplifying dynamics. When $H > 0.5$ ($FD < 1.5$), the time-series exhibits positive long-range correlations, and is more structured. The time-series displays a long-term trend, meaning past states influence future states.

There are four main properties that must be present for a time-series to be characterized by H or FD : 1) self-similarity; 2) power law scaling relationship; 3) scale-invariance; and 4) a scaling range (Figure 3). Each of these will be discussed in turn.

Self-similarity

Self-similarity means that pieces of the structure, when enlarged, resemble larger pieces or the whole (Figure 2 and Figure 3 A-C). Technically speaking, physiological time-series are self-affine, meaning their scaling is anisotropic (i.e. the proportions between enlarged pieces are different in one direction from those in the other). This is

277
278
279
280
281
282
283
284
285
286
287
288
289
290
291
292
293
294
295
296
297
298
299
300
301
302
303
304
305
306
307
308
309
310
311
312
313
314
315
316
317
318
319
320
321
322

323 because in one direction (time) the proportions between the enlarged pieces is different
324 than in the other (amplitude of signal; e.g. fMRI BOLD) [1].
325

326

327 **Power law scaling relationship**
328

329 Power law scaling means that, for a quantitative property, q , is measured in quantities
330 of s , its value depends on s according to the following scaling relationship:
331

332

333

334

335
$$q = f(s). \quad (2)$$

336

337

338 For non-fractal objects, the estimate of q using progressively smaller units of measure
339 s will converge to a single value as the size of the measurement units approaches zero.
340 On the other hand, fractals exhibit a power law scaling relationship with s , whereby
341 the estimated value of q increases without limit as the size of the s decreases.
342

343

344

345
$$q = ps^\epsilon \quad (3)$$

346

347

348 where p is a factor of proportionality (prefactor) and ϵ is a negative number, the
349 scaling exponent. The value of ϵ can be determined as the slope of the linear regression
350 fit to the data pairs on the plot of $\log q$ versus $\log s$:
351

352

353

354

355
$$\log q = \log p + \epsilon \log s \quad (4)$$

356

357

358 Data points for exact fractals will line up along perfectly with a linear-regression slope,
359 while statistical fractals will scatter around it since the two sides of Equation 4 are
360 equal only in distribution.
361

362

363

364

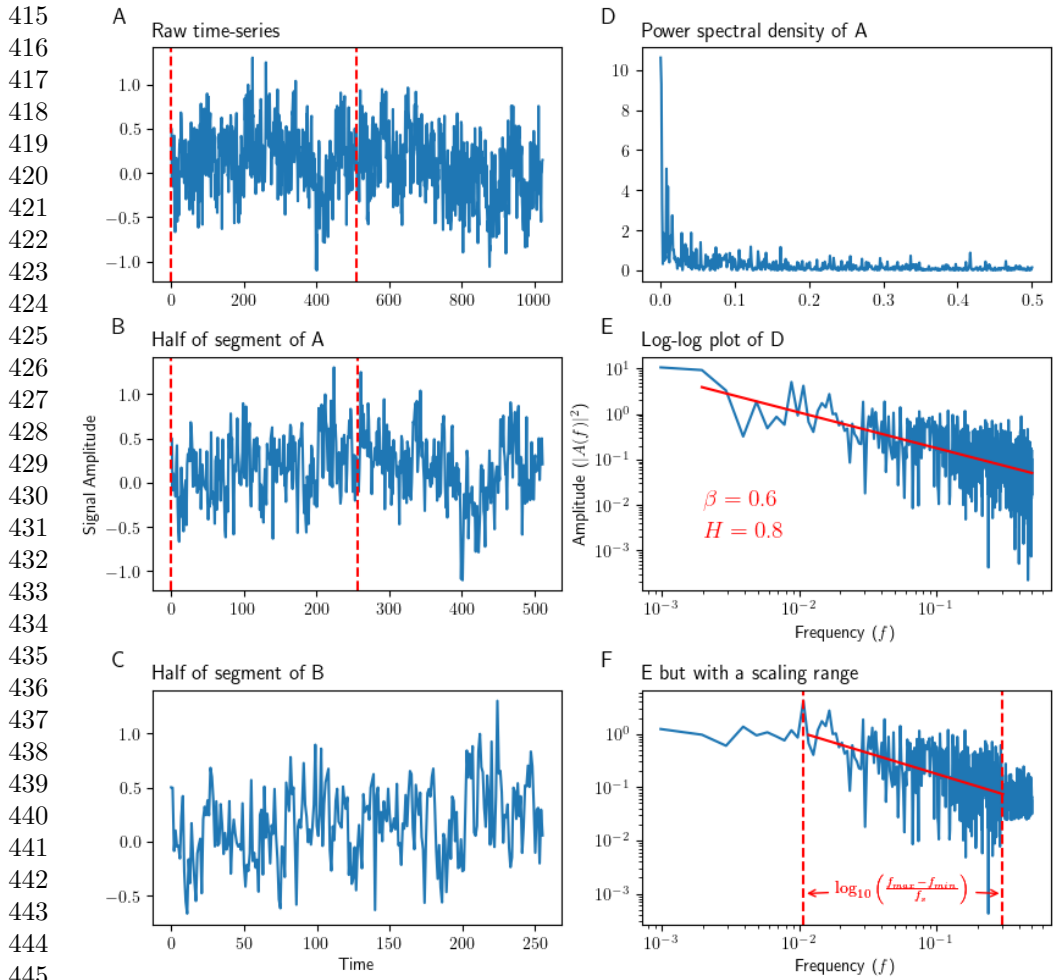
365

366

367

368

Scale-invariance	369
	370
The ratio of two estimates of q measured at two different scales, s_1 and s_2 , q_2/q_1	371
depends only on the ratio of scales (relative scale), s_2/s_1 , and not directly on the	372
absolute scale, s_1 or s_2	373
	374
	375
	376
	377
$q_2/q_1 = ps_2^\epsilon / ps_1^\epsilon = (s_2/s_1)^\epsilon \quad (5)$	378
	379
	380
For statistical fractals, like those of nature, s_2/s_1 may change in a continuous fashion	381
still leaving the validity of Equation 5 unaffected. The scale-invariance of fractals	382
arises from the fact that the geometrical structure only depends on the scaling factor	383
(ratio of scales), and not the absolute scale. As a result, quantitative properties of	384
smaller parts are similar to those of larger parts.	385
	386
	387
	388
	389
	390
Scaling range	391
	392
Natural fractals may only display scale-invariance within a restricted range, as they	393
are finite (either by definition or due to the fact that they must be sampled). The upper	394
cut-off point (s_{max}) in Equation 6, falls within the size range of the structure itself.	395
Similarly, the lower cut-off point (s_{min}) falls within the dimensions of the smallest	396
structural elements. The scaling range (SR) is defined in decades	397
	398
	399
	400
	401
	402
	403
$SR = \log_{10}(s_{max}/s_{min}) \quad (6)$	404
	405
	406
	407
	408
	409
	410
	411
	412
	413
	414



446 **Figure 3. Main properties of a fractal time-series** A-C show a raw time-series
 447 (fractional Gaussian noise in this example) at different scales: B is the first half of A
 448 (shown as vertical dashed lines in A), while C is half of B (shown in vertical dashed
 449 lines in B). D is a power spectral density plot of A. E shows D but on a log-log scale,
 450 demonstrating the linear nature of fractal signals when plotted on a log-log scale. The
 451 slope of E is $-\beta$. In this example, β is calculated to be 0.6, which translates to an
 452 H of 0.8. F shows a modified version of E, which imagines that E only demonstrates
 453 a power law scaling relationship between two distinct frequencies. The equation for
 454 calculating the scaling range in decades is shown. Exact fractal time-series (A) was
 455 created using the Davies-Harte method.

456
 457
 458
 459
 460

Prerequisites to measuring H	461
	462
Time-points	463
	464
	465
	466
	467
	468
	469
	470
	471
	472
	473
	474
	475
	476
	477
	478
	479
	480
	481
	482
Power-law scaling relationship	483
	484
	485
	486
	487
	488
	489
	490
	491
	492
	493
	494
	495
	496
	497
	498
	499
	500
	501
	502
	503
	504
	505
	506

507 [34, 35]). The 1,000 synthetic time-series are then converted to PSDs, and the KS
508 distance is again measured. The p -value is defined as the fraction of synthetic time
509 series with Ds that are larger than the D of the original time-series. The larger the p -
510 value, the more plausible the synthetic model (either fGn or fBm) is for representing
511 the original time-series, and the better the fit of the original data to a scale-free
512 distribution. The null-hypothesis that the time-series is not scale free is rejected if p
513 < 0.05 (i.e. if $p > 0.05$, we say that the time-series is scale-free).
514

515 It is important to note, however, that the p -value in question may need to be adjusted
516 based on the number of time-points.
517

518 A sample python code is provide in Section 2
519

520

521 **Scaling range**

522

523 As previously mentioned, statistical fractals are unlikely to display their power-law
524 scaling relationship across all scales. Therefore, it is important to test the scaling
525 relationship across a range of scales, determining the minimum and maximum scale
526 for which the scaling relationship exists (if at all). One way to determine this range
527 is to apply the power-law scaling test across a range of scales, starting with the full
528 range, and progressively reducing the size while trying to maintain the widest range.
529

530 However, this method can be computationally intensive, and prone to false negatives,
531 especially signals with very high or low H values. One solution is, instead of applying
532 this test to every voxel in a 4D fMRI brain scan, to segment the brain into separate
533 ROIs (e.g. anatomically based on an atlas, or functionally by first running ICA to
534 identify RSNs), average the time-series within each ROI, which will improve SNR,
535 and then run the power-law scaling test.
536

537

538 Once a scaling range is discovered, it is then important to use this range when mea-
539 suring H. For example, if H is being calculated using a frequency approach, the linear
540

regression can be limited to within the frequency range. However, if another approach
is used, a bandpass filter may be necessary first to remove unwanted frequencies. Care-
ful attention should be paid to the type of frequency filtering method employed, and
care must be taken not to re-introduce nuisance regressors previously removed [36].

Classification: Gaussian noise vs Brownian motion

If the prerequisites above have been met, the next step is to classify the signal type.
Fractal signals can be organized into two distinct kinds: fractional Gaussian noise
(fGn) and fractional Brownian motion (fBm) Figure 4. fGn signals are stationary,
meaning they tend to center along a mean and variance value over time. In contrast,
fBm signals are non-stationary: their values tend to wander away from the mean,
and their variance is a power function of the time span over which it is computed.
Curiously, fGn and fBm can easily be converted from one to the other: fGn to fBm
by applying a successive summation between elements of the fGn series; and fBm to
fGn by applying successive differences between elements of a fBm series.

When calculating the H of a signal, it is imperative to first classify the signal as either
fGn or fBm. Failure to do so can result in serious miscalculation of H, as different
estimators can produce extremely biased calculations depending on the assumed type
of signal. The distinction between fGn and fBm can be seen in their spectral properties.
Applying a Fourier transform of a signal to convert it from the time-domain to the
frequency domain, we can obtain a power spectral density, which relates the amplitude
of the frequency (y-axis) to the frequency (x-axis). The PSD of fGn signals follow
a power-law form: $|A(f)|^2 \propto f^{-\beta}$, where the exponent β ranges between -1 and 1.
This is known as $1/f$ noise, as the power is inversely proportional to frequency. fBm,
being a cumulative sum of fGn, has a different spectral behaviour: $|A(f)|^2 \propto f^{-(\beta+2)}$.
This steeper decay ($\beta + 2$) causes fBm to exhibit stronger low-frequency dominance,

599 making it distinct from $1/f$ noise. Thus, when $\beta \sim 1$, a signal is said to exist on the
600 $1/f$ boundary.

602

603 One method of calculating H, known as the spectral method or periodogram method
604 (PM), is based on the PSD. The PM method involves creating a log-log plot of the
605 time-series' periodogram using a fast Fourier transform (FFT; Figure 3 D and E),
606 calculating the linear-regression slope ($-\beta$), and, depending on the slope angle, using
607 one of two equations:

611

612

613

$$614 H = \begin{cases} \frac{\beta+1}{2}, & \text{if } -1 < \beta < 1 \\ 615 \frac{\beta-1}{2}, & \text{if } 1 < \beta < 3 \end{cases} \quad (7)$$

616

617

618

619

620

621

622

623

624

625

626

627

628

629

630

631

632

633

634

635

636

637

638

639

640

641

642

643

644

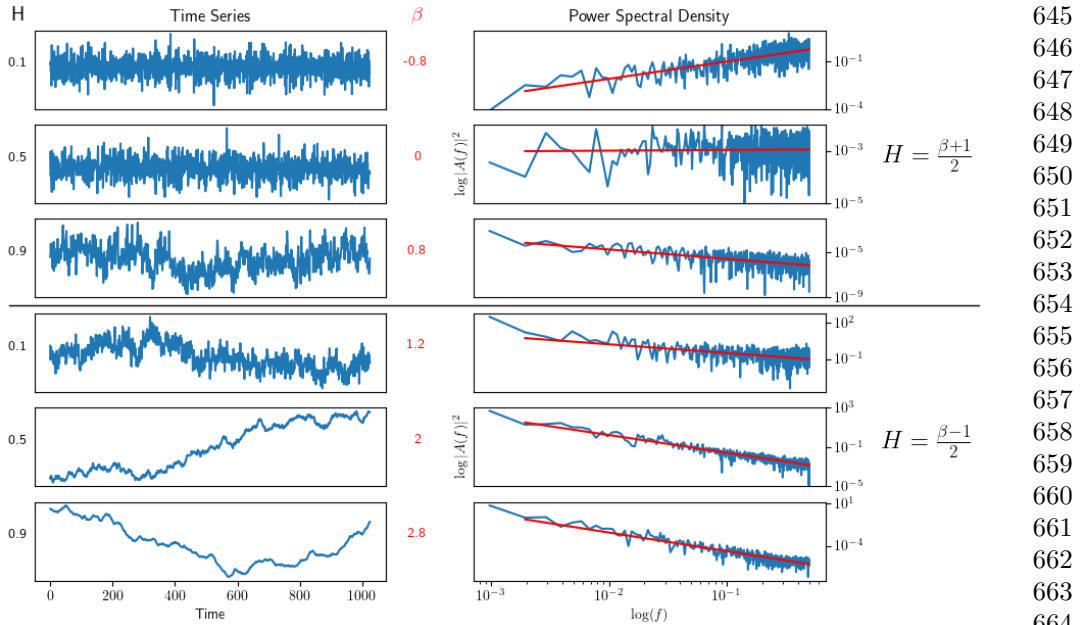


Figure 4. Simulated fractional Gaussian noise and fractional Brownian motion. Raw simulated time-series with 1,024 time-points and known Hurst values are plotted on the left. The top three time-series are fractional Gaussian noise, while the bottom three are fractional Brownian motion. H values are displayed on the left, while β values are displayed on the right. Note how fractional Gaussian noise remain centered around a mean (i.e. stationary), while fractional Brownian motion wanders away from the mean (i.e. non-stationary). Log-log power spectral density plots of the signals on the left are shown on the right. Linear-regression fits are shown in red, which are used to calculate β and H using the appropriate equation (on the right). Exact fractal time-series were created using the Davies-Harte method.

If the class of signal is not appropriately identified — for example, when β is ~ 1 — it is possible for a true $H \sim 0.9$ to be calculated as 0.1. Therefore, algorithms and research in properly classifying fractal signals is crucially important.

Several methods have been proposed for classifying fGn and fBm signals, including ones that make use of the PM described above [1, 17], detrended fluctuation analysis (DFA) [37], autoregressive fractionally integrated moving average (ARFIMA) [35], and

691 wavelet entropy [38, 39]. These methods, however, all struggle to distinguish signals
692 whose PSD β values are ~ 1 [1] (AKA the $1/f$ boundary).

694

695 fMRI Signals

696

697 Are fMRI signals expected to be fGn or fBm?

699

700 Measuring H

701

702 Fractal analysis tools vary in performance, assumptions, and limitations. In order
703 to avoid biasing ones results [Bassingthwaigte and Raymond [40]; @; @; @], it is
704 important to choose the right method carefully, especially when applied to physi-
705 ological signals which can be contaminated by unrelated noise. The following is a
706 non-exhaustive list of methods, and their relative strengths and weaknesses. Despite
707 their diversity, all approaches employ a version of scale-invariance analysis, by fitting
708 a log feature versus log scale for finding a scaling exponent from a regression slope,
709 and then calculating H from this scaling exponent. These methods, however, can be
710 subdivided into those that

711

712

713 • ARIMA (autoregressive integrated moving average) and ARFIMA (autoregressive
714 fractionally integrated moving- average)

715

716 • Adaptive fractal analysis (<https://www.frontiersin.org/journals/physiology/articles/10.3389/fphys.2020.00>)

717

718

719 Time-domain

720

721 *Rescaled range analysis (R/S)*

722

723

724

725 This is the original method used by Hurst in 1951 when studying hydrology and the
726 long term storage capacity of dams [20].

727

728

Dong et al. [41]	737
	738
<i>Dispersional analysis (DA)</i>	739
	740
	741
	742
	743
[42]	744
	745
Dona et al. [43] Dona et al. [44]	746
	747
	748
<i>Scaled window variance (SWV)</i>	749
	750
	751
	752
Dona et al. [43] Dona et al. [44]	753
	754
	755
<i>Generalized Hurst exponent (GHE)</i>	756
	757
	758
	759
	760
<i>Triangle total areas (TTA)</i>	761
	762
	763
	764
<i>Higuchi method (HM)</i>	765
	766
	767
	768
	769
<i>Central estimation (AM & AV)</i>	770
	771
	772
	773
<i>Detrended fluctuation analysis (DFA)</i>	774
	775
	776
	777
	778
<i>Least squares method via standard deviation (LSSD)</i>	779
	780
	781
	782

783 Bayesian
784
785
786 *Least squares method via variance (LSV)*
787
788
789
790 *Whittle's estimator (WE)*
791
792
793
794
795 Frequency-domain
796
797 *Periodogram method (PM)*
798
799
800
801 *Welch technique (PSD_{Welch})*
802
803
804
805
806 *Local Whittle (LW)*
807
808
809
810 Bayesian?
811
812
813 Mixture
814
815 *Average wavelet coefficient (AWC)*
816
817 <https://journals.aps.org/pre/abstract/10.1103/PhysRevE.58.2779>
818
819
820
821 *Variance vs level (VVL)*
822
823
824
825
826 *Maximum likelihood in the wavelet domain (MLW)*
827
828

Each fractal analysis tool has different performance, prerequisite conditions, and limitations, and each needs thorough evaluation in order to avoid bias or misinterpretation of the derived fractal parameters [5, 6, 8, 9], especially when applied to physiological signals which may be contaminated with noise [15, 28]. from [1] 829
830
831
832
833
834
835
836

Neuroscience Applications

H has emerged as a valuable tool in neuroscience and clinical research. Typically, H values reported in adult brains are above 0.5, with higher H values in grey matter than white matter or cerebrospinal fluid [41, 45]. Some key findings from neuroscience research include: a decrease in H during task performance [46, 47]; negative correlations with task novelty and difficulty [48]; increases with age in the frontal and parietal lobes [41], and hippocampus [49]; decreases with age in the insula, and limbic, occipital and temporal lobes [41]; H < 0.5 in preterm infants [50]; and more [51]. In terms of clinical findings, abnormal H values have been identified in Alzheimer's disease (AD) [52, 53], autism spectrum disorder (ASD) [43, 54–56], mild traumatic brain injury [44], major depressive disorder [57, 58] and schizophrenia [56, 59].

fMRI preprocessing considerations

Nuissance regression

When attempting to regress out non-BOLD signal, it is important to apply the regression at the same time, and not in succession. Even performing a band-pass filter after nuisance regression can re-introduce noise components [36].

Detrending

see Tanabe et al. [60]

875 **Hurst Reviews**

876

877 **Table**

878

879

880 **Table 1. fMRI-Hurst studies.** An attempt to gather all published fMRI studies
 881 that have used Hurst or Hurst-like analysis, some stats, and the main findings. Main
 882 findings are almost certainly more nuanced than how we have reported them here;
 883 we have attempted to condense the findings as succinctly as possible. n = number of
 884 subjects in the study; TR = repetition time; MLWD = maximum likelihood wavelet;
 885 PSD_{Welch} = power spectral density Welch method; DMN = default mode network;
 886 DFA = detrended fluctuation analysis; DA = dispersional analysis; SWV = scaled
 887 window variance; RS = rescaled range; LW = local Whittle;

888	Age				TR		
	889	Study	n	range	Methods	Volumes	(s)
890	Akhrif et al. (2018) [61]	103	19-28	AFA	task: 425, resting: 350	2	impulsivity: ↓
891	Barnes et al. (2009) [15]	14	21-29	MLW	2048	1.1	cognitive effort: ↓ H
892							
893							
894							
895							
896							
897							
898							
899							
900							
901							
902							
903							
904							
905							
906							
907							
908							
909							
910							
911							
912							
913							
914							
915							
916							
917							
918							
919							
920							

Study	n	Age		Methods	Volumes	(s)	TR	921
		range						922
Campbell et al. (2015) [62]	72	mean	PSD _{Welch}		900	1	movie-watching	923
		29					↑ H	924
							in	925
							visual,	926
							somatosensory,	927
							and	928
							dorsal	929
							sal	930
							attention;	931
							↓	932
							frontal	933
							topparietal	934
							and	935
							DMN	936
								937
								938
								939
								940
								941
								942
								943
								944
								945
								946
								947
								948
								949
								950
								951
								952
								953
								954
								955
								956
								957
								958
								959
								960
								961
								962
								963
								964
								965
								966

		Age				TR	
	Study	n	range	Methods	Volumes	(s)	Results
967	Churchill et al. (2015) [63]	97	n/a	DFA, Wavelet	285	1.5	worry: ↓ H
968		(28					
969			37				
970							
971							
972							
973							
974							
975							
976							
977							
978							
979							
980							
981							
982							
983							
984							
985							
986	Churchill et al. (2016) [48]	three	20-	DFA, PSD _{Welch}	~ 300	2	age, task nov-
987							
988							
989							
990							
991							
992							
993							
994							
995							
996							
997							
998							
999	Ciuciu et al. (2014) [46]	17	18-	Wavelet	194	2.16	networks
1000							
1001							
1002	Dona et al. (2017) [43]	71	mean	PSD, DA, SWV	300	2	ASD: ↑ H
1003							
1004							
1005							
1006							
1007							
1008							
1009							
1010							
1011							
1012							

Study	n	Age			Volumes	(s)	TR	Results
		range	Methods					
Dona et al. (2017) [44]	110 (55	mean 13	PSD, DA, SWV	180		2	mTBI: ↑ H	1013 1014 1015 1016 1017 1018 1019 1020 1021 1022 1023 1024
		mTBI: 55						
		HC)						
Dong et al. (2018) [41]	116	19- 85	RS	260		2.5	age: ↑ H frontal and pari- etal lobe; ↓ H insula, lim- bic, occip- ital, tem- poral lobes	1025 1026 1027 1028 1029 1030 1031 1032 1033 1034 1035 1036 1037 1038 1039 1040 1041 1042 1043 1044 1045 1046 1047 1048 1049 1050 1051 1052 1053 1054 1055 1056 1057 1058

1059	1060	1061	Age			TR			
			Study	n	range	Methods	Volumes	(s)	Results
1062			Drayne et al. (2024) [64]	98	preterm	PSD _{Welch}	100	3	preterm: ↓ H;
1063									dif-
1064									fer-
1065									enti-
1066									ates
1067									net-
1068									works
1069									
1070									
1071									
1072									
1073									
1074									
1075									
1076	Erbil et al. (2025) [65]	7	21-	28	Wavelet	1,000; 1,000, 3,000	1; 0.6; 0.2	microstates	
1077									
1078									
1079									
1080									
1081	Gao et al. (2018) [66]	110	mean	21	PSD, Wavelet	232	2	reappraisal	
1082									
1083									scores:
1084									↓ H
1085									
1086	Gao et al. (2023) [67]	195	18-	(100; 95)	Wavelet	?	2	rumination: ↑ H	
1087									
1088									
1089									
1090									
1091	Gentili et al. (2017) [68]	31	mean	25	Wavelet	512	1.64	neuroticism: ↓	
1092									
1093									
1094	Gentili et al. (2015) [69]	36	mean	27	Wavelet	450	2	social anxiety:	
1095									
1096									
1097									
1098									
1099									↑ H
1100									
1101									
1102									
1103									
1104									

Study	n	Age		Methods	Volumes	(s)	TR	Results	1105
		range							1106
Guan et al. (2024) [70]	31	21-		multifractal	160	1.9	ADHD,	1109	1107
	HC	50	DFA				BP,	1110	1108
		and					SZ:	1111	1106
	31						mul-	1112	1113
		ADHD;					ti-	1115	1114
	34						frac-	1117	1116
	HC						tal	1118	1119
	and						reduc-	1120	1121
	34						tion	1122	1123
	BP;						in	1124	1125
	42						bell-	1125	1126
	HC						shaped	1127	1128
	and						asym-	1129	1130
	42						me-	1130	1131
	SCHZ						try	1132	1133
								1134	1135
								1135	1136
								1136	1137
								1137	1138
								1138	1139
								1139	1140
								1140	1141
								1141	1142
								1142	1143
								1143	1144
								1144	1145
								1145	1146
								1146	1147
								1147	1148
								1148	1149
								1149	1150

			Age			TR	
	Study	n	range	Methods	Volumes	(s)	Results
1151							
1152							
1153	He et al. (2011) [47]	17	18- 27	DFA, PSD	194	2.16	task: ↓ H;
1154							
1155							dif-
1156							fer-
1157							enti-
1158							ates
1159							net-
1160							works;
1161							brain
1162							glu-
1163							cose
1164							metabolism
1165							and
1166							neu-
1167							rovas-
1168							cular
1169							cou-
1170							pling
1171							
1172							Jager et
1173							al. (2023) [71]
1174							(20
1175							32
1176							task;
1177							
1178							20 no
1179							
1180							task)
1181							
1182							
1183							
1184							
1185							
1186							
1187							
1188							
1189							
1190							
1191							
1192							
1193							
1194							
1195							
1196							

Study	n	Age		Methods	Volumes	TR (s)	Results	1197
		range						1198
Lai et al. (2010) [54]	63	n/a		Wavelet	512	1.3	ASD: ↓ H	1199
		(33						1200
		ASD;						1201
		3-						1202
		HC)						1203
Lei et al. (2013) [72]	17	18-		Wavelet	200	1.5	extroversion: ↓ H	1204
		29						1205
							in	1206
							DMN	1207
Lei et al. (2021) [73]	75	mean	RS		240	2	moyamoya:	1208
	(16	~ 41					dis-	1209
			HMMD;				ease:	1210
			34				↓ H	1211
								1212
			IMMD;					1213
			25					1214
								1215
			HC)					1216
Linke et al. (2024) [55]	83	1.5-5	WML		400	0.8	age of chil- dren ASD: ↓ H in vmPFC	1227
								1228
								1229
								1230
								1231
								1232
								1233
								1234
								1235
								1236
								1237
								1238
								1239
								1240
								1241
								1242

1243	Age				TR		
	1244 1245 Study	n	range	Methods	Volumes	(s)	Results
1246							
1247	Maxim et al. (2005) [52]	21	n/a	LW, Wornell, MLW	150	2	AD: ↑ H
1248							
1249							
1250	Mella et al. (2024) [50]	716	preterm	PSD _{Welch}	2,300	0.392	preterm: ↓ H;
1251							H
1252							starts
1253							< 0.5
1254							at
1255							preterm
1256							age ;
1257							dif-
1258							fer-
1259							enti-
1260							ates
1261							net-
1262							works
1263							
1264							
1265							
1266							
1267							
1268							
1269							
1270							
1271							
1272							
1273							
1274							
1275							
1276							
1277							
1278							
1279							
1280							
1281							
1282							
1283							
1284							
1285							
1286							
1287							
1288							

Study	n	Age		Methods	Volumes	TR (s)	Results	1289
		range						1290
Omidvarnia et al. (2021) [74]	100	22-35		PSD, DFA	min 250	0.72	cognitive load: ↓ H; H and entropy-based complexity highly correlated; H high-est in fronto-toparietal net-work and default mode	1291 1292 1293 1294 1295 1296 1297 1298 1299 1300 1301 1302 1303 1304 1305 1306 1307 1308 1309 1310 1311 1312 1313 1314 1315 1316 1317 1318 1319 1320 1321 1322 1323 1324 1325 1326 1327 1328 1329 1330 1331 1332 1333 1334

		Age				TR	
	Study	n	range	Methods	Volumes	(s)	Results
1335							
1336							
1337	Rubin et al. (2013) [75]	22	?	Many	?	?	HFFT and PSD _{Welch}
1338							
1339							
1340							
1341							
1342							
1343							
1344							out-
1345							per-
1346							form
1347							other
1348							meth-
1349							ods
1350							
1351							
1352							
1353							
1354	Sokunbi et al. (2014) [59]	29	?	DA, DFA	?	?	SZ: ↓ H
1355							
1356			(13				
1357			SZ;				
1358							
1359			16				
1360				HC)			
1361							
1362	Suckling et al. (2008) [16]	22	22	MLW	512	1.1	multifractal
1363							
1364			(11	and			reanal-
1365			old;	65			ysis
1366							
1367			11				of
1368				young)			
1369							[49]
1370	Tetereva et al. (2020)	23	mean	DFA	300	2	fear: ↓ H
1371							
1372				23.9			
1373							then
1374							
1375							↑ H
1376							
1377							
1378							
1379							
1380							

Study	n	Age		Methods	Volumes	TR		Results
		range	(s)			(s)	Results	
Uscătescu et al. (2023) [56]	124	?	Wavelet	947?	0.475	ASD	1381 1382 1383 1384 1385 1386 1387 1388 1389 1390 1391 1392 1393 1394 1395	
	(55					and		
	TD;					SZ: ↓	1388 1389	
	30					H	1390 1391 1392 1393 1394 1395	
	AT;							
	39							
	SZ)							
Varley et al. (2020) [76]	33	?	HFD	?	?	Lower	1396 1397 1398 1399 1400 1401 1402 1403 1404 1405 1406 1407 1408 1409 1410 1411 1412 1413 1414 1415 1416 1417 1418 1419 1420 1421 1422 1423 1424 1425 1426	
	(15					con-		
	HC;					sciou-	1398 1399	
	10					ness:	1400 1401 1402	
	min					↓ H	1403 1404	
	con-						1405	
	sciou;						1406	
	8						1407	
	veg)						1408 1409 1410 1411 1412 1413 1414 1415 1416 1417 1418 1419 1420 1421 1422 1423 1424 1425 1426	

		Age				TR	
	Study	n	range	Methods	Volumes	(s)	Results
1427							
1428							
1429	Study	n	range	Methods	Volumes	(s)	Results
1430							
1431	von Wegner et	?	?	Wavelet, DFA	1500	2.08	multiscale
1432	al. (2018) [77]						vari-
1433							ance
1434							effects
1435							pro-
1436							duce
1437							Hurst
1438							phe-
1439							nom-
1440							ena
1441							with-
1442							out
1443							long-
1444							range
1445							depen-
1446							dence
1447							
1448							
1449							
1450							
1451							
1452							
1453							
1454							
1455							
1456							
1457	Warsi et	46	?	PSD, RD	2,400	0.25	AD:
1458	al. (2012) [53]	(33					↑ H
1459							
1460							
1461			AD;				
1462			13				
1463							
1464			HC)				
1465							
1466							
1467							
1468							
1469							
1470							
1471							
1472							

Study	n	Age		Methods	Volumes	(s)	TR	Results
		range						
Weber et al. (2014) [78]	14	22-38		Wavelet	512	2	acute alcohol hol intoxica- tion: mix of uparrow and downarrow H	1473 1474 1475 1476 1477 1478 1479 1480 1481 1482 1483 1484 1485 1486 1487 1488 1489 1490 1491 1492 1493 1494 1495 1496 1497 1498 1499 1500 1501 1502 1503 1504 1505 1506 1507 1508 1509 1510 1511 1512 1513 1514 1515 1516 1517 1518

		Age				TR	
	Study	n	range	Methods	Volumes	(s)	Results
1519							
1520							
1521							
1522							
1523	Wink et	22	22	MLW	512	1.1	age:
1524	al. (2006) [49]	(11	and				↑ H
1525		old;	65				in
1526							bilat-
1527			11				
1528							
1529			young)				eral
1530							
1531							hip-
1532							
1533							pocam-
1534							pus;
1535							scopo-
1536							
1537							lamine:
1538							
1539							↑ H;
1540							
1541							faster
1542							
1543							task:
1544							
1545							↑ H
1546	Wink et	11	mean	Wavelet	136	1.1	latency
1547	al. (2008) [45]		35 ±				
1548							in
1549			10				fame
1550							
1551							deci-
1552							
1553							sion
1554							
1555							task:
1556							
1557							↓ H
1558	Xie et	70	?	Wavelet	700	0.6	pharmac-
1559	al. (2024) [79]						resistant
1560							
1561							TLE:
1562							
1563							↓ H
1564							

Nonparametric trend estimation in the presence of fractal noise:	1565
Application to fMRI time-series analysis - Afshinpour et al. (2008)	1566
[80]	1567
	1568
	1569
	1570
	1571
	1572
	1573
	1574
	1575
	1576
	1577
	1578
	1579
	1580
	1581
	1582
	1583
	1584
	1585
	1586
	1587
	1588
	1589
	1590
	1591
	1592
	1593
	1594
	1595
	1596
	1597
	1598

In this paper, a method for estimating trend in the presence of fractal noise is proposed and applied to fMRI time-series. To this end, a partly linear model (PLM) is fitted to each time-series. The parametric and nonparametric parts of PLM are considered as contributions of hemodynamic response and trend, respectively. Using the whitening property of wavelet transform, the unknown components of the model are estimated in the wavelet domain. The results of the proposed method are compared to those of other parametric trend-removal approaches such as spline and polynomial models. It is shown that the proposed method improves activation detection and decreases variance of the estimated parameters relative to the other methods.

Notes:

- trend estimation paper
- 1.5T, 3.9x3.9x6mm, 1.648s TR, 256 time-points
- Hurst method: Wavelet db4 with 5 scales

Fractal Analysis of BOLD time-series in a Network Associated With Waiting Impulsivity - Akhrif et al. (2018) [61]

examined **103** healthy male students at **rest** and while performing the 5-choice serial reaction time **task**. We addressed fractality in a network associated with waiting impulsivity using the **adaptive fractal analysis (AFA)** approach to determine H. We revealed the fractal nature of the impulsivity network. Furthermore, fractality was influenced by individual impulsivity in terms of decreasing fractality (H) with higher impulsivity in regions of top-down control (left middle frontal gyrus) as well as reward processing (nucleus accumbens and anterior cingulate cortex).

```

1611 Notes:
1612
1613
1614 • fMRI split into low and high frequency components. LFC is the second order
1615 polynomial that is a smooth and global fit of the original time course.
1616
1617 • AFA: variance of fluctuation computed around, in this case, a second order
1618 polynomial trend  $v(i)$  fitted to time-series within each segment  $w$ , and its size:
1619
1620
1621
1622 
$$F(w) = \sqrt{\frac{1}{N} \sum_{i=1}^N (u(i) - v(i))^2} \sim w^H \quad (8)$$

1623
1624
1625
1626  $N$ : length of the time-series
1627
1628
1629
1630  $w = 2n + 1, n = 5, 6..., 13$ 
1631
1632
1633  $H$  is determined as the slope of the log-log plot  $\log_2(F(w))$  as a function of  $\log_2(w)$ 
1634
1635 Example code:
1636
1637 #| echo: true
1638 #| code-fold: true
1639 #| code-summary: "Code"
1640
1641 import numpy as np
1642
1643
1644
1645
1646 def adaptive_fractal_analysis(signal, n_values=range(5, 14)):
1647     """
1648         Perform Adaptive Fractal Analysis (AFA) to compute the Hurst exponent.
1649
1650
1651         Parameters:
1652             signal (array-like): time-series data to analyze.
1653
1654
1655
1656

```

```

n_values (iterable): Sequence of `n` values to define window sizes1657 as  $w = 2n + 1$ .
    1658
    1659
    1660
    1661
    1662
    1663
    1664
    1665
    1666
    1667
    1668
    1669
    1670
    1671
    1672
    1673
    1674
    1675
    1676
    1677
    1678
    1679
    1680
    1681
    1682
    1683
    1684
    1685
    1686
    1687
    1688
    1689
    1690
    1691
    1692
    1693
    1694
    1695
    1696
    1697
    1698
    1699
    1700
    1701
    1702

Returns:
    float: Estimated Hurst exponent (H).

"""

# Define window sizes as w = 2n + 1

window_sizes = [2 * n + 1 for n in n_values]
fluctuations = []

for window_size in window_sizes:
    segment_variances = []
    for start in range(0, len(signal) - window_size + 1, window_size):
        # Extract the window
        window = signal[start:start + window_size]
        # Fit a second-order polynomial (quadratic fit) and compute residual
        x = np.arange(len(window))
        p = np.polyfit(x, window, deg=2) # Degree 2 polynomial
        residual = window - np.polyval(p, x)
        # Compute variance of the residuals
        variance = np.var(residual)
        segment_variances.append(variance)

    # Compute average variance for this window size
    fluctuations.append(np.mean(segment_variances))

# Fit the scaling law: log(fluctuations) vs. log(window_sizes)
log_window_sizes = np.log(window_sizes)

```

```

1703     log_fluctuations = np.log(fluctuations)
1704
1705     slope, intercept = np.polyfit(log_window_sizes, log_fluctuations, deg=1)
1706
1707
1708     # The slope corresponds to the Hurst exponent
1709
1710     return slope
1711
1712
1713 Endogenous human brain dynamics recover slowly following
1714
1715 cognitive effort - Barnes et al. (2009) [15]
1716
1717     1) Does performance of a cognitively effortful task significantly change fractal
1718         scaling properties of fMRI time-series compared to their values before task per-
1719         formance? 2) If so, can we relate the extent of task-related perturbation to the
1720         difficulty of the task? This result supports the model that endogenous low fre-
1721         quency oscillatory dynamics are relevant to the brain's response to exogenous
1722         stimulation. Moreover, it suggests that large-scale neurocognitive systems mea-
1723         sured using fMRI, like the heart and other physiological systems subjected to
1724         external demands for enhanced performance, can take a considerable period of
1725         time to return to a stable baseline state.
1731
1732
1733 Notes:
1734
1735
1736     • maximum likelihood in the wavelet domain
1737
1738
1739 Wavelets and functional magnetic resonance imaging of the human
1740 brain - Bullmore et al. (2004) [81]
1741
1742
1743     We provide a brief formal introduction to key properties of the DWT and review the
1744     growing literature on its application to fMRI. We focus on three applications in particular:
1745     (i) wavelet coefficient resampling or "wavestrapping" of 1-D time-series, 2- to 3-D spatial
1746
1747
1748

```

maps and 4-D spatiotemporal processes; (ii) wavelet-based estimators for signal and noise parameters of time-series regression models assuming the errors are fractional Gaussian noise (fGn); and (iii) wavelet shrinkage in frequentist and Bayesian frameworks to support multiresolution hypothesis testing on spatially extended statistic maps. 1749
1750
1751
1752
1753
1754
1755
1756
1757
1758
1759
1760
1761
1762
1763

Notes:

- This paper suggests that motion correction translates many fBm signals to fGn...
however, it is not clear where this data comes from.

Fractal-Based Analysis of fMRI BOLD Signal During Naturalistic Viewing Conditions - Campbell et al. (2021) [62]

We performed fractal analysis on Human Connectome Project 7T fMRI data ($n = 72$, 41 females, mean age 29.46 ± 3.76 years) to compare H across movie-watching and rest. Results: In contrast to previous work using conventional tasks, we found higher H values for movie relative to rest (mean difference = 0.014; $p = 5.279 \times 10^{-7}$; 95% CI [0.009, 0.019]). H was significantly higher in movie than rest in the visual, somatomotor and dorsal attention networks, but was significantly lower during movie in the frontoparietal and default networks. We found no cross-condition differences in test-retest reliability of H. Finally, we found that H of movie-derived stimulus properties (e.g., luminance changes) were fractal whereas H of head motion estimates were non-fractal.

Notes:

-

1795 Scale-free brain dynamics under physical and psychological distress:

1796

1797 Pre-treatment effects in women diagnosed with breast cancer -

1798

1799 Churchill et al. (2015) [63]

1800

1801 In a BOLD functional magnetic resonance imaging study, we scanned three groups during a
1802 working memory task: women scheduled to receive chemotherapy or radiotherapy and aged-
1803 matched controls. Surprisingly, patients' BOLD signal exhibited greater H with increasing
1804 intensity of anticipated treatment. However, an analysis of H and functional connectivity
1805 against self-reported measures of psychological distress (Worry, Anxiety, Depression) and
1806 physical distress (Fatigue, Sleep problems) revealed significant interactions. The modula-
1807 tion of (Worry, Anxiety) versus (Fatigue, Sleep Problems, Depression) showed the strongest
1808 effect, where higher worry and lower fatigue was related to reduced H in regions involved
1809 in visuospatial search, attention, and memory processing. This is also linked to decreased
1810 functional connectivity in these brain regions.

1811

1812

1813 Notes:

1814

1815

1816

1817 The suppression of scale-free fMRI brain dynamics across three

1818

1819 different sources of effort: Aging, task novelty and task difficulty -

1820

1821 Churchill et al. (2016) [48]

1822

1823 Decreases in the Hurst exponent (H), which quantifies scale-free signal, was related to three
1824 different sources of cognitive effort/task engagement: 1) task difficulty, 2) task novelty,
1825 and 3) aging effects. These results were consistently observed across multiple datasets
1826 and task paradigms. We also demonstrated that estimates of H are robust across a range
1827 of time-window sizes. H was also compared to alternative metrics of BOLD variability
1828 (SDBOLD) and global connectivity (Gconn), with effort-related decreases in H producing
1829 similar decreases in SDBOLD and Gconn.

1830

1831

1832 Notes:

1833

1834

1835

Interplay between functional connectivity and scale-free dynamics in intrinsic fMRI networks - Ciuciu et al. (2014) [46]

We applied this framework to fMRI data acquired from healthy young adults at rest and performing a visual detection task. First, we found that scale-invariance existed beyond univariate dynamics, being present also in bivariate cross-temporal dynamics. Second, we observed that frequencies within the scale-free range do not contribute evenly to interregional connectivity, with a systematically stronger contribution of the lowest frequencies, both at rest and during task. Third, in addition to a decrease of the Hurst exponent and inter-regional correlations, task performance modified cross-temporal dynamics, inducing a larger contribution of the highest frequencies within the scale-free range to global correlation. Lastly, we found that across individuals, a weaker task modulation of the frequency contribution to inter-regional connectivity was associated with better task performance manifesting as shorter and less variable reaction times. These findings bring together two related fields that have hitherto been studied separately – resting-state networks and scale-free dynamics, and show that scale-free dynamics of human brain activity manifest in cross-regional interactions as well.

Notes:

Temporal fractal analysis of the rs-BOLD signal identifies brain abnormalities in autism spectrum disorder - Dona et al. (2017) [43]

“It is important to mention here that fractal dimension estimation based on a dispersional analysis is quite robust with respect to uncorrelated noise and does not require preprocessing”

Notes:

- ASD = reduced FD = increased H;
- rare study to properly define fGn vs fBm first?

1887 Fractal analysis of brain blood oxygenation level dependent (BOLD)
1888
1889 signals from children with mild traumatic brain injury (mTBI) -

1890
1891 Dona et al. (2017) [44]

1892
1893 Notes:

1894

1895

1896 • children with mTBI; mTBI = reduced FD = increased H

1897 • rare study to properly define fGn vs fBm first?
1898

1899

1900 Hurst Exponent Analysis of Resting-State fMRI Signal Complexity
1901

1902 across the Adult Lifespan - Dong et al. (2018) [41]
1903

1904 Region-wise and voxel-wise analyses were performed to investigate the effects of age, gen-
1905 der, and their interaction on complexity. In region-wise analysis, we found that the healthy
1906 aging is accompanied by a loss of complexity in frontal and parietal lobe and increased
1907 complexity in insula, limbic, and temporal lobe. Meanwhile, differences in HE between gen-
1908 ders were found to be significant in parietal lobe ($p = 0.04$, corrected). However, there was
1909 no interaction between gender and age. In voxel-wise analysis, the significant complexity
1910 decrease with aging was found in frontal and parietal lobe, and complexity increase was
1911 found in insula, limbic lobe, occipital lobe, and temporal lobe with aging. Meanwhile, dif-
1912 ferences in HE between genders were found to be significant in frontal, parietal, and limbic
1913 lobe. Furthermore, we found age and sex interaction in right parahippocampal gyrus ($p =$
1914 0.04, corrected). Our findings reveal HE variations of the rs-fMRI signal across the human
1915 adult lifespan and show that HE may serve as a new parameter to assess healthy aging
1916 process.
1917

1918

1919 Notes:

1920

1921

1922 • They state that increase in age = decrease in complexity
1923

1924

1925

1926

Pitfalls in fractal time-series analysis: fMRI BOLD as an exemplary case - Eke et al. (2012) [82]	1933 1934 1935 1936 1937 1938 1939
Wavelet-Generalized Least Squares: A New BLU Estimator of Linear Regression Models with 1/f Errors - Fadili & Bullmore (2002) [83]	1940 1941 1942 1943 1944 1945 1946
Not in one metric: Neuroticism modulates different resting state metrics within distinctive brain regions - Gentili et al. (2017) [68]	1947 1948 1949 1950 1951 1952 1953 1954 1955 1956 1957 1958 1959 1960
Metrics more related to the measurement of regional intrinsic brain activity (fALFF, ALFF and REHO), or that provide a parsimonious index of integrated and segregated brain activity (HE), were more broadly modulated in regions related to emotions and their regulation. Metrics related to connectivity were modulated across a wider network of areas. Overall, these results show that neuroticism affects distinct aspects of brain resting state activity.	1961 1962 1963 1964 1965 1966 1967 1968 1969 1970 1971 1972 1973 1974 1975 1976 1977 1978
Notes:	
• “parsimonious index of integrated and segregated brain activity (HE)”	
• HE was inversely correlated to neuroticism	
Proneness to social anxiety modulates neural complexity in the absence of exposure: A resting state fMRI study using Hurst exponent - Gentili et al. (2015) [69]	
Results from fALFF were highly consistent with those obtained using LSAS and BFNE to predict HE. Overall our data indicate that spontaneous brain activity is influenced by the degree of social anxiety, on a continuum and in the absence of social stimuli. These	

1979 findings suggest that social anxiety is a trait characteristic that shapes brain activity and
1980 predisposes to different reactions in social contexts.
1981

1982

1983 **Notes:**

1984

1985

1986

- 1987 • “A recent article (Rubin et al., 2013) analyzes the robustness of different algorithms
1988 with respect to possible fMRI artifacts and time-series lengths. In particular, the
1989 relevance of preprocessing steps as motion correction, detrending and filtering were
1990 evaluated both on simulated and real fMRI data, while other preprocessing steps
1991 like segmentation were not evaluated, although they may have an impact on”
1992
- 1993 • “The HE of fMRI time-series is generally higher in gray matter than in white matter
1994 (Maxim et al., 2005), augments in the hippocampus with aging, and decreases with
1995 cholinergic transmission enhancement (Wink et al., 2006)”
1996
- 1997 • “As pointed out by Maxim (Maxim et al., 2005), fMRI noise, after these pre-
1998 processing steps, can be described as fGn.”
1999

2000

2001

2002

2003

2004

2005

2006

2007

2008

2009

2010

2011

2012

2013

2014

2015

2016

2017

2018

2019

2020

2021

2022

2023

2024

Real-time fractal signal processing in the time domain. - Hartmann et al. (2013) [84] 2025
2026
2027
2028

Here we introduce real-time variants of the Detrended Fluctuation Analysis (DFA) and the closely related Signal Summation Conversion (SSC) methods, which are suitable to estimate the fractal exponent in one pass.

Altered fractal dynamics of gait: Reduced stride-interval correlations with aging and Huntington's disease. - Hausdoff et al. (1997) [85] 2029
2030
2031
2032
2033
2034

Notes: 2035
2036
2037
2038

- Gait... not fMRI 2039
2040
2041

Scale-Free Properties of the Functional Magnetic Resonance Imaging Signal during Rest and Task - He (2011) [47] 2042
2043
2044

its power-law exponent differentiates between brain networks and correlates with fMRI signal variance and brain glucose metabolism. Importantly, in parallel to brain electrical field potentials, the variance and power-law exponent of the fMRI signal decrease during task activation, suggesting that the signal contains more long-range memory during rest and conversely is more efficient at online information processing during task. The scale-free properties of the fMRI signal and brain electrical field potentials bespeak their respective stationarity and nonstationarity. This suggests that neurovascular coupling mechanism is likely to contain a transformation from nonstationarity to stationarity.

The fMRI signal time course from each ROI was extracted for each subject and fMRI run. The normalized or non-normalized power spectrum of the fMRI signal was computed using the Bartlett smoothing procedure of deriving the power spectral function from the lagged autocorrelation or auto-covariance function, respectively (Jenkins and Watts, 1998). A Tukey window of 20 fMRI frame width was applied for additional smoothing. The power

2071 spectra were then averaged across runs and subjects and across homologous ROIs, resulting
2072 in an average power spectrum for each of 21 brain regions (Fig. 2A). Finally, to obtain the
2073 power-law exponent , the <0.1 Hz range of each average power spectrum was fit with a
2074 power-law function: $P(f) \sim 1/f$ using a least-squares fit. Using the low-frequency range to
2075 fit the power-law exponent avoids aliasing artifact in higher-frequency range (we used TR
2076 of 2.16 s, hence Nyquist limit is 0.23 Hz) and yields reliable measurement of the scale-free
2077 distribution (Eke et al., 2002).

2081

2082

2083 The DFA method has the particular advantage of being applicable to both stationary and
2084 nonstationary data. To analyze our fMRI data, window lengths of 5, 10, 19, 38, and 95
2085 fMRI frames were chosen so that the number of frames in each run (190 after discarding
2086 the first four frames) is an integer multiple of the window length.

2088

2089

2090 **Fractal characterization of complexity in dynamic signals:**

2091 **Application to cerebral hemodynamics - Herman (2009) [13]**

2093

2094 **Identification of brain activity from fMRI data: Comparison of three**
2095 **fractal scaling analyses. - Hu (2006) [86]**

2097

2098 **A shift to randomness of brain oscillations in people with autism.**

2099

2100 **Lai (2010) [54]**

2102

2103 Complex fractal scaling of fMRI time-series was found in both groups but globally there
2104 was a significant shift to randomness in the ASC (mean $H = .758$, $SD = .045$) compared
2105 with neurotypical volunteers (mean $H = .788$, $SD = .047$).

2107

2108

2109

2110

2111

2112

2113

2114

2115

2116

Extraversion is encoded by scale-free dynamics of default mode network. Lei (2013) [72]	2117 2118 2119 2120
Fractional Gaussian noise, functional MRI and Alzheimer's disease. Maxim (2005) [52]	2121 2122 2123 2124
we adopted the Davies-Harte algorithm, which is both exact and fast, to generate the fGn simulations used here. For each value of $H = 0.1, \dots, 0.9$, we simulated 1000 realizations of fGn with 512 time-points in each series; we set $\omega^2 = 1$ for all simulations.	2125 2126 2127 2128 2129 2130
NOTES:	2131 2132 2133
• This paper has the figure showing signal goes from fBm to fGn with proper motion regression	2134 2135 2136 2137 2138
Decomposing multifractal crossovers. Nagy (2017) [87]	2139 2140 2141 2142 2143 2144 2145 2146 2147 2148 2149 2150 2151 2152
The NIRS and fMRI-BOLD low-frequency fluctuations were dominated by a multifractal component over an underlying biologically relevant random noise, thus forming a bimodal signal. The crossover between the EEG signal components was found at the boundary between the α and β bands, suggesting an independent generator for the multifractal rhythm. The robust implementation of the SFD method should be regarded as essential in the seamless processing of large volumes of bimodal fMRI-BOLD imaging data for the topology of multifractal metrics free of the masking effect of the underlying random noise.	2153 2154 2155 2156 2157 2158 2159 2160 2161 2162
Optimizing complexity measures for FMRI data: Algorithm, artifact, and sensitivity. Rubin (2013) [75]	2153 2154 2155 2156 2157 2158 2159 2160 2161 2162
Power-spectrum, Higuchi's fractal dimension, and generalized Hurst exponent based estimates were most successful by all criteria; the poorest-performing measures were wavelet, detrended fluctuation analysis, aggregated variance, and rescaled range. Our results clearly demonstrate that decisions regarding choice of algorithm, signal processing, time-series	2153 2154 2155 2156 2157 2158 2159 2160 2161 2162

length, and scanner have a significant impact on the reliability and sensitivity of complexity estimates. operating on the edge of chaos, complex systems position themselves for optimal responsivity to inputs, as well as ability to maintain homeostatic regulation. Daubechies wavelet based computations (Hdb) *have long computation times, are not sensitive to spikes, and show poor sensitivity to activation, tissue type, and emotional content; for these Daubechies wavelet based estimates the overall performance increases with the wavelet order up to a point (Hdb8), and then deteriorates.* HRS and HAV, performed poorly across the board. In terms of image contrast, overlap with activation, and group differences, HDFA performed poorly as well, with HDFA-S outperforming HDFA and HDFA-L, suggesting that the bulk of useful information is found at shorter lags. The most consistently successful measures were the powerspectrum based measures HFFT and HpWelch, with the latter slightly outperforming the former while taking much longer to compute Second, it appears that detrending, regressing out the global mean, and excluding low frequencies improves agreement between complexity and activation. 300-600 time-points Finally, the best measures to use are either the power-spectrum based ones (HFFT or HpWelch) on a restricted frequency range (above ,0.01 Hz),

2188
2189 **Mutual information identifies spurious Hurst phenomena in resting**
2190
2191 **state EEG and fMRI data. von Wegner (2018) [77]**

2192 In these processes, which do not have long-range memory by construction, a spurious Hurst
2193 phenomenon occurs due to slow relaxation times and heteroscedasticity (time-varying con-
2194 ditional variance). In summary, we find that mutual information correctly distinguishes
2195 long-range from short-range dependence in the theoretical and experimental cases dis-
2196 cussed. Our results also suggest that the stationary fGn process is not sufficient to describe
2197 neural data, which seem to belong to a more general class of stochastic processes, in which
2198 multiscale variance effects produce Hurst phenomena without long-range dependence. In
2199 our experimental data, the Hurst phenomenon and long-range memory appear as different
2200 system properties that should be estimated and interpreted independently.
2201
2202
2203
2204
2205
2206
2207
2208

References	2209
	2210
[1] Eke A, Hermán P, Bassingthwaigte J, Raymond G, Percival D, Cannon M, et al.	2211
Physiological Time Series: Distinguishing Fractal Noises from Motions. Pflügers	2212
Archiv - European Journal of Physiology. 2000 Feb;439(4):403–415. https://doi.org/10.1007/s004249900135 .	2213
	2214
	2215
	2216
	2217
	2218
[2] Koch HV. Sur Une Courbe Continue sans Tangente, Obtenue Par Une	2219
Construction Géométrique Élémentaire. Astron och Fys. 1904;1:681–702.	2220
	2221
	2222
[3] Koch H. Une Méthode Géométrique Élémentaire Pour l'étude de Certaines Ques-	2223
tions de La Théorie Des Courbes Planes. Acta Mathematica. 1906;30(0):145–174.	2224
https://doi.org/10.1007/BF02418570 .	2225
	2226
	2227
	2228
[4] Mandelbrot B. How Long Is the Coast of Britain? Statistical Self-Similarity and	2229
Fractional Dimension. Science. 1967 May;156(3775):636–638. https://doi.org/10.1126/science.156.3775.636 .	2230
	2231
	2232
	2233
	2234
[5] Jayalalitha G, Shanthoshini Deviha V, Uthayakumar R. Fractal Model for	2235
Blood Flow in Cardiovascular System. Computers in Biology and Medicine. 2008	2236
Jun;38(6):684–693. https://doi.org/10.1016/j.combiomed.2008.03.002 .	2237
	2238
	2239
[6] Ansell HS, Kovács IA. Unveiling Universal Aspects of the Cellular Anatomy of	2240
the Brain. Communications Physics. 2024 Jun;7(1):184. https://doi.org/10.1038/s42005-024-01665-y .	2241
	2242
	2243
	2244
	2245
[7] Riley MA, Bonnette S, Kuznetsov N, Wallot S, Gao J. A Tutorial Introduction	2246
to Adaptive Fractal Analysis. Frontiers in Physiology. 2012;3. https://doi.org/10.3389/fphys.2012.00371 .	2247
	2248
	2249
	2250
	2251
	2252
	2253
	2254

- 2255 [8] Csermely P. Weak Links: Stabilizers of Complex Systems from Proteins to Social
2256 Networks. 1st ed. The Frontiers Collection. Berlin New York: Springer; 2006.
2257
- 2258
- 2259 [9] Bak P, Tang C, Wiesenfeld K. Self-Organized Criticality: An Explanation of the
2260 1/ f Noise. Physical Review Letters. 1987 Jul;59(4):381–384. [https://doi.org/10.](https://doi.org/10.1103/PhysRevLett.59.381)
2261 [1103/PhysRevLett.59.381](https://doi.org/10.1103/PhysRevLett.59.381).
- 2262
- 2263
- 2264
- 2265 [10] Lipsitz LA. Loss of 'Complexity' and Aging: Potential Applications of Fractals
2266 and Chaos Theory to Senescence. JAMA. 1992 Apr;267(13):1806. [https://doi.](https://doi.org/10.1001/jama.1992.03480130122036)
2267 [org/10.1001/jama.1992.03480130122036](https://doi.org/10.1001/jama.1992.03480130122036).
- 2268
- 2269
- 2270
- 2271 [11] Lipsitz LA. Dynamics of Stability: The Physiologic Basis of Functional Health
2272 and Frailty. The Journals of Gerontology Series A: Biological Sciences and Med-
2273 ical Sciences. 2002 Mar;57(3):B115–B125. [https://doi.org/10.1093/gerona/57.3.](https://doi.org/10.1093/gerona/57.3.B115)
2274 [B115](https://doi.org/10.1093/gerona/57.3.B115).
- 2275
- 2276
- 2277
- 2278 [12] Beggs JM. The Cortex and the Critical Point. 1st ed. Cambridge, MA: MIT
2279 Press Direct; 2022.
- 2280
- 2281
- 2282 [13] Herman P, Kocsis L, Eke A. Fractal Characterization of Complexity in Dynamic
2283 Signals: Application to Cerebral Hemodynamics. In: Walker JM, Hyder F, editors.
2284 2285 Dynamic Brain Imaging. vol. 489. Totowa, NJ: Humana Press; 2009. p. 23–40.
- 2286
- 2287
- 2288 [14] Werner G. Fractals in the Nervous System: Conceptual Implications for Theoret-
2289 ical Neuroscience. Frontiers in Physiology. 2010;[https://doi.org/10.3389/fphys.](https://doi.org/10.3389/fphys.2010.00015)
2290 [2010.00015](https://doi.org/10.3389/fphys.2010.00015).
- 2291
- 2292
- 2293
- 2294 [15] Barnes A, Bullmore ET, Suckling J. Endogenous Human Brain Dynamics Recover
2295 Slowly Following Cognitive Effort. PLoS ONE. 2009 Aug;4(8):e6626. [https://doi.](https://doi.org/10.1371/journal.pone.0006626)
2296 [org/10.1371/journal.pone.0006626](https://doi.org/10.1371/journal.pone.0006626).
- 2297
- 2298
- 2299
- 2300

- [16] Suckling J, Wink AM, Bernard FA, Barnes A, Bullmore E. Endogenous Multifractal Brain Dynamics Are Modulated by Age, Cholinergic Blockade and Cognitive Performance. *Journal of Neuroscience Methods*. 2008 Sep;174(2):292–300. <https://doi.org/10.1016/j.jneumeth.2008.06.037>. 2301
2302
2303
2304
2305
2306
2307
2308
2309
2310
2311
2312
2313
2314
2315
2316
2317
2318
2319
2320
2321
2322
2323
2324
2325
2326
2327
2328
2329
2330
2331
2332
2333
2334
2335
2336
2337
2338
2339
2340
2341
2342
2343
2344
2345
2346
- [17] Eke A, Herman P, Kocsis L, Kozak LR. Fractal Characterization of Complexity in Temporal Physiological Signals. *Physiological Measurement*. 2002 Feb;23(1):R1–R38. <https://doi.org/10.1088/0967-3334/23/1/201>. 2308
2309
2310
2311
2312
2313
2314
2315
2316
2317
2318
2319
2320
2321
2322
2323
2324
2325
2326
2327
2328
2329
2330
2331
2332
2333
2334
2335
2336
2337
2338
2339
2340
2341
2342
2343
2344
2345
2346
- [18] Hermán P, Kocsis L, Eke A. Fractal Branching Pattern in the Pial Vasculature in the Cat. *Journal of Cerebral Blood Flow and Metabolism: Official Journal of the International Society of Cerebral Blood Flow and Metabolism*. 2001 Jun;21(6):741–753. <https://doi.org/10.1097/00004647-200106000-00012>. 2314
2315
2316
2317
2318
2319
2320
2321
2322
2323
2324
2325
2326
2327
2328
2329
2330
2331
2332
2333
2334
2335
2336
2337
2338
2339
2340
2341
2342
2343
2344
2345
2346
- [19] Taylor R. Personal Reflections on Jackson Pollock’s Fractal Paintings. *História, Ciências, Saúde-Manguinhos*. 2006 Oct;13(suppl):109–123. <https://doi.org/10.1590/S0104-59702006000500007>. 2321
2322
2323
2324
2325
2326
2327
2328
2329
2330
2331
2332
2333
2334
2335
2336
2337
2338
2339
2340
2341
2342
2343
2344
2345
2346
- [20] Hurst HE. Long-Term Storage Capacity of Reservoirs. *Transactions of the American Society of Civil Engineers*. 1951 Jan;116(1):770–799. <https://doi.org/10.1061/TACEAT.0006518>. 2321
2322
2323
2324
2325
2326
2327
2328
2329
2330
2331
2332
2333
2334
2335
2336
2337
2338
2339
2340
2341
2342
2343
2344
2345
2346
- [21] Mandelbrot B. Une Classe de Processus Stochastiques Homothetiques Soi: Application a Loi Climatologique de H. E. Hurst. *Comptes Rendus Del academie Des Sciences De Paris*. 1965;240:3274–3277. 2321
2322
2323
2324
2325
2326
2327
2328
2329
2330
2331
2332
2333
2334
2335
2336
2337
2338
2339
2340
2341
2342
2343
2344
2345
2346
- [22] Molz FJ, Liu HH, Szulga J. Fractional Brownian Motion and Fractional Gaussian Noise in Subsurface Hydrology: A Review, Presentation of Fundamental Properties, and Extensions. *Water Resources Research*. 1997 Oct;33(10):2273–2286. <https://doi.org/10.1029/97WR01982>. 2321
2322
2323
2324
2325
2326
2327
2328
2329
2330
2331
2332
2333
2334
2335
2336
2337
2338
2339
2340
2341
2342
2343
2344
2345
2346

- 2347 [23] Korvin G. Fractal Models in the Earth Sciences. Amsterdam ; New York: Elsevier;
2348
2349 1992.
- 2350
- 2351 [24] Park K, Willinger W, editors. Self-Similar Network Traffic and Performance
2352
2353 Evaluation. 1st ed. Wiley; 2000.
- 2354
- 2355 [25] Graves T, Gramacy R, Watkins N, Franzke C. A Brief History of Long Mem-
2356
2357 ory: Hurst, Mandelbrot and the Road to ARFIMA, 1951–1980. Entropy. 2017
2358 Sep;19(9):437. <https://doi.org/10.3390/e19090437>.
- 2360
- 2361 [26] Shannon CE. Communication in the Presence of Noise. Proceedings of the IRE.
2362
2363 1949 Jan;37(1):10–21. <https://doi.org/10.1109/JRPROC.1949.232969>.
- 2364
- 2365 [27] Clauset A, Shalizi CR, Newman MEJ. Power-Law Distributions in Empiri-
2366
2367 cal Data. SIAM Review. 2009 Nov;51(4):661–703. <https://doi.org/10.1137/070710111>.
- 2370
- 2371 [28] Kolmogorov A. Sulla Determinazione Empirica Di Una Legge Di Distribuzione.
2372
2373 Giornale dell’Istituto Italiano degli Attuari. 1933;4:83–91.
- 2374
- 2375 [29] Smirnov N. Table for Estimating the Goodness of Fit of Empirical Distributions.
2376
2377 The Annals of Mathematical Statistics. 1948 Jun;19(2):279–281. <https://doi.org/10.1214/aoms/1177730256>.
- 2380
- 2381 [30] Peitgen HO. The Science of Fractal Images. New York, NY: Springer New York;
2382
2383 1988.
- 2384
- 2385 [31] Davies RB, Harte DS. Tests for Hurst Effect. Biometrika. 1987;74(1):95–101.
2386
2387 <https://doi.org/10.1093/biomet/74.1.95>.
- 2388
- 2389 [32] Asmussen S. Stochastic Simulation with a View Towards Stochastic Processes.
2390
2391 University of Aarhus, Centre for Mathematical Physics and Stochastics; 1998.
- 2392

- [33] Hosking JR. Modeling Persistence in Hydrological Time Series Using Fractional Differencing. *Water Resources Research*. 1984;20(12):1898–1908. 2393
2394
2395
2396
2397
2398
2399
2400
2401
2402
2403
2404
2405
2406
2407
2408
2409
- [34] Roume C, Ezzina S, Blain H, Delignières D. Biases in the Simulation and Analysis of Fractal Processes. *Computational and Mathematical Methods in Medicine*. 2019 Dec;2019:1–12. <https://doi.org/10.1155/2019/4025305>. 2400
2401
2402
2403
2404
2405
2406
2407
2408
2409
- [35] Granger CWJ, Joyeux R. AN INTRODUCTION TO LONG-MEMORY TIME SERIES MODELS AND FRACTIONAL DIFFERENCING. *Journal of Time Series Analysis*. 1980 Jan;1(1):15–29. <https://doi.org/10.1111/j.1467-9892.1980.tb00297.x>. 2403
2404
2405
2406
2407
2408
2409
- [36] Lindquist MA, Geuter S, Wager TD, Caffo BS. Modular Preprocessing Pipelines Can Reintroduce Artifacts into fMRI Data. *Human Brain Mapping*. 2019 Jun;40(8):2358–2376. <https://doi.org/10.1002/hbm.24528>. 2410
2411
2412
2413
2414
2415
- [37] Peng CK, Mietus J, Hausdorff JM, Havlin S, Stanley HE, Goldberger AL. Long-Range Anticorrelations and Non-Gaussian Behavior of the Heartbeat. *Physical Review Letters*. 1993 Mar;70(9):1343–1346. <https://doi.org/10.1103/PhysRevLett.70.1343>. 2416
2417
2418
2419
2420
2421
2422
2423
2424
2425
2426
2427
2428
2429
2430
- [38] Ramirez Pacheco J, Torres Román D, Toral Cruz H. Distinguishing Stationary/Nonstationary Scaling Processes Using Wavelet Tsallis q -Entropies. *Mathematical Problems in Engineering*. 2012 Jan;2012(1):867042. <https://doi.org/10.1155/2012/867042>. 2431
2432
2433
2434
2435
2436
2437
2438
- [39] Ramírez-Pacheco J, Trejo-Sánchez J, Cortez-González J, Palacio R. Classification of Fractal Signals Using Two-Parameter Non-Extensive Wavelet Entropy. *Entropy*. 2017 May;19(5):224. <https://doi.org/10.3390/e19050224>. 2431
2432
2433
2434
2435
2436
2437
2438

- 2439 [40] Bassingthwaighte JB, Raymond GM. Evaluating Rescaled Range Analysis for
2440 Time Series. Annals of Biomedical Engineering. 1994 Jul;22(4):432–444. <https://doi.org/10.1007/BF02368250>.
- 2441
2442
2443
2444
2445 [41] Dong J, Jing B, Ma X, Liu H, Mo X, Li H. Hurst Exponent Analysis of
2446 Resting-State fMRI Signal Complexity across the Adult Lifespan. Frontiers in
2447 Neuroscience. 2018 Feb;12:34. <https://doi.org/10.3389/fnins.2018.00034>.
- 2448
2449
2450
2451 [42] Bassingthwaighte J. Physiological Heterogeneity: Fractals Link Determinism and
2452 Randomness in Structures and Functions. Physiology. 1988 Feb;3(1):5–10. <https://doi.org/10.1152/physiologyonline.1988.3.1.5>.
- 2453
2454
2455
2456 [43] Dona O, Hall GB, Noseworthy MD. Temporal Fractal Analysis of the Rs-BOLD
2457 Signal Identifies Brain Abnormalities in Autism Spectrum Disorder. PLOS ONE.
2458 2017 Dec;12(12):e0190081. <https://doi.org/10.1371/journal.pone.0190081>.
- 2459
2460
2461
2462 [44] Dona O, Noseworthy MD, DeMatteo C, Connolly JF. Fractal Analysis of Brain
2463 Blood Oxygenation Level Dependent (BOLD) Signals from Children with Mild
2464 Traumatic Brain Injury (mTBI). PLOS ONE. 2017 Jan;12(1):e0169647. <https://doi.org/10.1371/journal.pone.0169647>.
- 2465
2466
2467
2468
2469
2470 [45] Wink AM, Bullmore E, Barnes A, Bernard F, Suckling J. Monofractal and Multi-
2471 fractal Dynamics of Low Frequency Endogenous Brain Oscillations in Functional
2472 MRI. Human Brain Mapping. 2008 Jul;29(7):791–801. <https://doi.org/10.1002/hbm.20593>.
- 2473
2474
2475
2476
2477 [46] Ciuciu P, Abry P, He BJ. Interplay between Functional Connectivity and Scale-
2478 Free Dynamics in Intrinsic fMRI Networks. NeuroImage. 2014 Jul;95:248–263.
2479 <https://doi.org/10.1016/j.neuroimage.2014.03.047>.
- 2480
2481
2482
2483
2484

- [47] He BJ. Scale-Free Properties of the Functional Magnetic Resonance Imaging Signal during Rest and Task. *The Journal of Neuroscience*. 2011 Sep;31(39):13786–13795. <https://doi.org/10.1523/JNEUROSCI.2111-11.2011>. 2485
2486
2487
2488
2489
2490
2491
2492
2493
2494
2495
2496
2497
2498
2499
2500
2501
2502
2503
2504
2505
2506
2507
2508
2509
2510
2511
2512
2513
2514
2515
2516
2517
2518
2519
2520
2521
2522
2523
2524
2525
2526
2527
2528
2529
2530
- [48] Churchill NW, Spring R, Grady C, Cimprich B, Askren MK, Reuter-Lorenz PA, et al. The Suppression of Scale-Free fMRI Brain Dynamics across Three Different Sources of Effort: Aging, Task Novelty and Task Difficulty. *Scientific Reports*. 2016 Aug;6(1):30895. <https://doi.org/10.1038/srep30895>. 2490
2491
2492
2493
2494
2495
2496
2497
2498
2499
2500
2501
2502
2503
2504
2505
2506
2507
2508
2509
2510
2511
2512
2513
2514
2515
2516
2517
2518
2519
2520
2521
2522
2523
2524
2525
2526
2527
2528
2529
2530
- [49] Wink AM, Bernard F, Salvador R, Bullmore E, Suckling J. Age and Cholinergic Effects on Hemodynamics and Functional Coherence of Human Hippocampus. *Neurobiology of Aging*. 2006 Oct;27(10):1395–1404. <https://doi.org/10.1016/j.neurobiolaging.2005.08.011>. 2498
2499
2500
2501
2502
2503
2504
2505
2506
2507
2508
2509
2510
2511
2512
2513
2514
2515
2516
2517
2518
2519
2520
2521
2522
2523
2524
2525
2526
2527
2528
2529
2530
- [50] Mella AE, Vanderwal T, Miller SP, Weber AM. Temporal Complexity of the BOLD-signal in Preterm versus Term Infants. *Cerebral Cortex*. 2024 Oct;34(10):bhae426. <https://doi.org/10.1093/cercor/bhae426>. 2500
2501
2502
2503
2504
2505
2506
2507
2508
2509
2510
2511
2512
2513
2514
2515
2516
2517
2518
2519
2520
2521
2522
2523
2524
2525
2526
2527
2528
2529
2530
- [51] Campbell OL, Weber AM. Monofractal Analysis of Functional Magnetic Resonance Imaging: An Introductory Review. *Human Brain Mapping*. 2022 Jun;43(8):2693–2706. <https://doi.org/10.1002/hbm.25801>. 2500
2501
2502
2503
2504
2505
2506
2507
2508
2509
2510
2511
2512
2513
2514
2515
2516
2517
2518
2519
2520
2521
2522
2523
2524
2525
2526
2527
2528
2529
2530
- [52] Maxim V, Šendur L, Fadili J, Suckling J, Gould R, Howard R, et al. Fractional Gaussian Noise, Functional MRI and Alzheimer’s Disease. *NeuroImage*. 2005 Mar;25(1):141–158. <https://doi.org/10.1016/j.neuroimage.2004.10.044>. 2500
2501
2502
2503
2504
2505
2506
2507
2508
2509
2510
2511
2512
2513
2514
2515
2516
2517
2518
2519
2520
2521
2522
2523
2524
2525
2526
2527
2528
2529
2530
- [53] Warsi MA, Molloy W, Noseworthy MD. Correlating Brain Blood Oxygenation Level Dependent (BOLD) Fractal Dimension Mapping with Magnetic Resonance Spectroscopy (MRS) in Alzheimer’s Disease. *Magnetic Resonance Materials in Physics, Biology and Medicine*. 2012 Oct;25(5):335–344. <https://doi.org/10.1007/s00119-012-1131-2>. 2500
2501
2502
2503
2504
2505
2506
2507
2508
2509
2510
2511
2512
2513
2514
2515
2516
2517
2518
2519
2520
2521
2522
2523
2524
2525
2526
2527
2528
2529
2530

- 2531 s10334-012-0312-0.
2532
2533 [54] Lai MC, Lombardo MV, Chakrabarti B, Sadek SA, Pasco G, Wheelwright SJ,
2534 et al. A Shift to Randomness of Brain Oscillations in People with Autism. Biological
2535 Psychiatry. 2010 Dec;68(12):1092–1099. <https://doi.org/10.1016/j.biopsych.2010.06.027>.
2536
2537
2538
2539
2540
2541 [55] Linke AC, Chen B, Olson L, Cordova M, Wilkinson M, Wang T, et al.
2542 Altered Development of the Hurst Exponent in the Medial Prefrontal Cortex in
2543 Preschoolers With Autism. Biological Psychiatry: Cognitive Neuroscience and
2544 Neuroimaging. 2024 Sep;p. S2451902224002714. <https://doi.org/10.1016/j.bpsc.2024.09.003>.
2545
2546
2547
2548
2549
2550 [56] Uscătescu LC, Hyatt CJ, Dunn J, Kronbichler M, Calhoun V, Corbera S, et al.:
2551 Using the Excitation/Inhibition Ratio to Optimize the Classification of Autism
2552 and Schizophrenia.
2553
2554
2555
2556 [57] Wei M, Qin J, Yan R, Li H, Yao Z, Lu Q. Identifying Major Depressive Disorder
2557 Using Hurst Exponent of Resting-State Brain Networks. Psychiatry Research:
2558 Neuroimaging. 2013 Dec;214(3):306–312. <https://doi.org/10.1016/j.psychresns.2013.09.008>.
2559
2560
2561
2562
2563 [58] Jing B, Long Z, Liu H, Yan H, Dong J, Mo X, et al. Identifying Current
2564 and Remitted Major Depressive Disorder with the Hurst Exponent: A Compar-
2565 ative Study on Two Automated Anatomical Labeling Atlases. Oncotarget. 2017
2566 Oct;8(52):90452–90464. <https://doi.org/10.18632/oncotarget.19860>.
2567
2568
2569
2570
2571 [59] Sokunbi MO, Gradin VB, Waiter GD, Cameron GG, Ahearn TS, Murray AD,
2572 et al. Nonlinear Complexity Analysis of Brain fMRI Signals in Schizophre-
2573 nia. PLoS ONE. 2014 May;9(5):e95146. <https://doi.org/10.1371/journal.pone.0095146>.

- [60] Tanabe J, Miller D, Tregellas J, Freedman R, Meyer FG. Comparison of Detrending Methods for Optimal fMRI Preprocessing. *NeuroImage*. 2002 Apr;15(4):902–907. <https://doi.org/10.1006/nimg.2002.1053>. 2577
2578
2579
2580
2581
2582
2583
2584
2585
2586
2587
2588
2589
- [61] Akhrif A, Romanos M, Domschke K, Schmitt-Boehrer A, Neufang S. Fractal Analysis of BOLD Time Series in a Network Associated With Waiting Impulsivity. *Frontiers in Physiology*. 2018 Oct;9:1378. <https://doi.org/10.3389/fphys.2018.01378>. 2583
2584
2585
2586
2587
2588
2589
- [62] Campbell O, Vanderwal T, Weber AM. Fractal-Based Analysis of fMRI BOLD Signal During Naturalistic Viewing Conditions. *Frontiers in Physiology*. 2022 Jan;12:809943. <https://doi.org/10.3389/fphys.2021.809943>. 2590
2591
2592
2593
2594
2595
- [63] Churchill NW, Cimprich B, Askren MK, Reuter-Lorenz PA, Jung MS, Peltier S, et al. Scale-free Brain Dynamics under Physical and Psychological Distress: Pre-treatment Effects in Women Diagnosed with Breast Cancer. *Human Brain Mapping*. 2015 Mar;36(3):1077–1092. <https://doi.org/10.1002/hbm.22687>. 2596
2597
2598
2599
2600
2601
2602
2603
2604
2605
2606
2607
2608
2609
2610
- [64] Drayne JP, Mella AE, McLean MM, Ufkes S, Chau V, Guo T, et al. Long-Range Temporal Correlation Development in Resting-State fMRI Signal in Preterm Infants: Scanned Shortly after Birth and at Term-Equivalent Age. *PLOS Complex Systems*. 2024 Dec;1(4):e0000024. <https://doi.org/10.1371/journal.pcsy.0000024>. 2611
2612
2613
2614
2615
2616
2617
2618
2619
2620
2621
2622
- [65] Erbil N, Deshpande G. Scale-Free Dynamics of Resting-State fMRI Microstates. *Fractal and Fractional*. 2025 Feb;9(2):112. <https://doi.org/10.3390/fractfract9020112>.
- [66] Gao W, Chen S, Biswal B, Lei X, Yuan J. Temporal Dynamics of Spontaneous Default-Mode Network Activity Mediate the Association between Reappraisal and Depression. *Social Cognitive and Affective Neuroscience*. 2018 Oct;<https://doi.org/10.1080/17435030.2018.1491111>. 2617
2618
2619
2620
2621
2622

- 2623 [//doi.org/10.1093/scan/nsy092](https://doi.org/10.1093/scan/nsy092).
- 2624
- 2625 [67] Gao W, Biswal B, Yang J, Li S, Wang Y, Chen S, et al. Temporal Dynamic
2626 Patterns of the Ventromedial Prefrontal Cortex Underlie the Association between
2627 Rumination and Depression. *Cerebral Cortex*. 2023 Feb;33(4):969–982. <https://doi.org/10.1093/cercor/bhac115>.
- 2631
- 2632
- 2633 [68] Gentili C, Cristea IA, Ricciardi E, Vanello N, Popita C, David D, et al. Not in One
2634 Metric: Neuroticism Modulates Different Resting State Metrics within Distinctive
2635 Brain Regions. *Behavioural Brain Research*. 2017 Jun;327:34–43. <https://doi.org/10.1016/j.bbr.2017.03.031>.
- 2639
- 2640 [69] Gentili C, Vanello N, Cristea I, David D, Ricciardi E, Pietrini P. Proneness to
2641 Social Anxiety Modulates Neural Complexity in the Absence of Exposure: A Rest-
2642 ing State fMRI Study Using Hurst Exponent. *Psychiatry Research: Neuroimaging*.
2644 2015 May;232(2):135–144. <https://doi.org/10.1016/j.pscychresns.2015.03.005>.
- 2646
- 2647
- 2648 [70] Guan S, Zhang Z, Meng C, Biswal B. Multifractal Dynamic Changes of
2649 Spontaneous Brain Activity in Psychiatric Disorders: Adult Attention Deficit-
2650 Hyperactivity Disorder, Bipolar Disorder, and Schizophrenia. *Journal of Affective
2651 Disorders*. 2025 Mar;373:291–305. <https://doi.org/10.1016/j.jad.2025.01.007>.
- 2653
- 2654
- 2655 [71] Jäger ATP, Bailey A, Huntenburg JM, Tardif CL, Villringer A, Gauthier CJ,
2656 et al. Decreased Long-range Temporal Correlations in the RESTING-STATE FUNC-
2657 TIONAL MAGNETIC RESONANCE IMAGING BLOOD-OXYGEN-LEVEL-DEPENDENT
2659 Signal Reflect Motor Sequence Learning up to 2 Weeks Following Training.
2660 Human Brain Mapping. 2024 Mar;45(4):e26539. <https://doi.org/10.1002/hbm.26539>.
- 2664
- 2665
- 2666
- 2667
- 2668

- [72] Lei X, Zhao Z, Chen H. Extraversion Is Encoded by Scale-Free Dynamics of Default Mode Network. *NeuroImage*. 2013 Jul;74:52–57. <https://doi.org/10.1016/j.neuroimage.2013.02.020>. 2669
2670
2671
2672
2673
2674
2675
2676
2677
2678
2679
2680
2681
2682
2683
2684
2685
2686
2687
2688
2689
2690
2691
2692
2693
2694
2695
2696
2697
2698
2699
2700
2701
2702
2703
2704
2705
2706
2707
2708
2709
2710
2711
2712
2713
2714
- [73] Lei Y, Li Y, Yu L, Xu L, Zhang X, Zheng G, et al. Faded Critical Dynamics in Adult Moyamoya Disease Revealed by EEG and fMRI. *Oxidative Medicine and Cellular Longevity*. 2021 Jan;2021(1):6640108. <https://doi.org/10.1155/2021/6640108>. 2669
2670
2671
2672
2673
2674
2675
2676
2677
2678
2679
2680
2681
2682
2683
2684
2685
2686
2687
2688
2689
2690
2691
2692
2693
2694
2695
2696
2697
2698
2699
2700
2701
2702
2703
2704
2705
2706
2707
2708
2709
2710
2711
2712
2713
2714
- [74] Omidvarnia A, Liégeois R, Amico E, Preti MG, Zalesky A, Van De Ville D.: Assessment of Temporal Complexity in Functional MRI between Rest and Task Conditions. *Bioengineering*. 2669
2670
2671
2672
2673
2674
2675
2676
2677
2678
2679
2680
2681
2682
2683
2684
2685
2686
2687
2688
2689
2690
2691
2692
2693
2694
2695
2696
2697
2698
2699
2700
2701
2702
2703
2704
2705
2706
2707
2708
2709
2710
2711
2712
2713
2714
- [75] Rubin D, Fekete T, Mujica-Parodi LR. Optimizing Complexity Measures for fMRI Data: Algorithm, Artifact, and Sensitivity. *PLoS ONE*. 2013 May;8(5):e63448. <https://doi.org/10.1371/journal.pone.0063448>. 2669
2670
2671
2672
2673
2674
2675
2676
2677
2678
2679
2680
2681
2682
2683
2684
2685
2686
2687
2688
2689
2690
2691
2692
2693
2694
2695
2696
2697
2698
2699
2700
2701
2702
2703
2704
2705
2706
2707
2708
2709
2710
2711
2712
2713
2714
- [76] Varley TF, Craig M, Adapa R, Finoia P, Williams G, Allanson J, et al. Fractal Dimension of Cortical Functional Connectivity Networks & Severity of Disorders of Consciousness. *PLOS ONE*. 2020 Feb;15(2):e0223812. <https://doi.org/10.1371/journal.pone.0223812>. 2669
2670
2671
2672
2673
2674
2675
2676
2677
2678
2679
2680
2681
2682
2683
2684
2685
2686
2687
2688
2689
2690
2691
2692
2693
2694
2695
2696
2697
2698
2699
2700
2701
2702
2703
2704
2705
2706
2707
2708
2709
2710
2711
2712
2713
2714
- [77] Von Wegner F, Laufs H, Tagliazucchi E. Mutual Information Identifies Spurious Hurst Phenomena in Resting State EEG and fMRI Data. *Physical Review E*. 2018 Feb;97(2):022415. <https://doi.org/10.1103/PhysRevE.97.022415>. 2669
2670
2671
2672
2673
2674
2675
2676
2677
2678
2679
2680
2681
2682
2683
2684
2685
2686
2687
2688
2689
2690
2691
2692
2693
2694
2695
2696
2697
2698
2699
2700
2701
2702
2703
2704
2705
2706
2707
2708
2709
2710
2711
2712
2713
2714
- [78] Weber AM, Soreni N, Noseworthy MD. A Preliminary Study on the Effects of Acute Ethanol Ingestion on Default Mode Network and Temporal Fractal Properties of the Brain. *Magnetic Resonance Materials in Physics, Biology and Medicine*. 2014 Aug;27(4):291–301. <https://doi.org/10.1007/s10334-013-0420-5>. 2669
2670
2671
2672
2673
2674
2675
2676
2677
2678
2679
2680
2681
2682
2683
2684
2685
2686
2687
2688
2689
2690
2691
2692
2693
2694
2695
2696
2697
2698
2699
2700
2701
2702
2703
2704
2705
2706
2707
2708
2709
2710
2711
2712
2713
2714

- 2715 [79] Xie K, Royer J, Rodriguez-Cruces R, Horwood L, Ngo A, Arafat T, et al.:
2716 Pharmaco-Resistant Temporal Lobe Epilepsy Gradually Perturbs the Cortex-
2717 Wide Excitation-Inhibition Balance.
2719
2720
2721 [80] Afshinpour B, Hosseini-Zadeh GA, Soltanian-Zadeh H. Nonparametric Trend
2722 Estimation in the Presence of Fractal Noise: Application to fMRI Time-Series
2723 Analysis. Journal of Neuroscience Methods. 2008 Jun;171(2):340–348. <https://doi.org/10.1016/j.jneumeth.2008.03.017>.
2725
2726
2727
2728 [81] Bullmore E, Fadili J, Maxim V, Şendur L, Whitcher B, Suckling J, et al. Wavelets
2729 and Functional Magnetic Resonance Imaging of the Human Brain. NeuroImage.
2730 2004 Jan;23:S234–S249. <https://doi.org/10.1016/j.neuroimage.2004.07.012>.
2731
2732
2733
2734 [82] Eke A. Pitfalls in Fractal Time Series Analysis: fMRI BOLD as an Exemplary
2735 Case. Frontiers in Physiology. 2012;3. <https://doi.org/10.3389/fphys.2012.00417>.
2736
2737
2738 [83] Fadili MJ, Bullmore ET. Wavelet-Generalized Least Squares: A New BLU
2739 Estimator of Linear Regression Models with 1/f Errors. NeuroImage. 2002
2740 Jan;15(1):217–232. <https://doi.org/10.1006/nimg.2001.0955>.
2741
2742
2743
2744 [84] Hartmann A, Mukli P, Nagy Z, Kocsis L, Hermán P, Eke A. Real-Time Fractal
2745 Signal Processing in the Time Domain. Physica A: Statistical Mechanics and its
2746 Applications. 2013 Jan;392(1):89–102. <https://doi.org/10.1016/j.physa.2012.08.002>.
2747
2748
2749
2750
2751
2752 [85] Hausdorff JM, Mitchell SL, Firtion R, Peng CK, Cudkowicz ME, Wei JY,
2753 et al. Altered Fractal Dynamics of Gait: Reduced Stride-Interval Correlations
2754 with Aging and Huntington’s Disease. Journal of Applied Physiology. 1997
2755 Jan;82(1):262–269. <https://doi.org/10.1152/jappl.1997.82.1.262>.
2756
2757
2758
2759
2760

- [86] Hu J, Lee J, Gao J, White KD, Crosson B. Identification of Brain Activity from fMRI Data: Comparison of Three Fractal Scaling Analyses. In: 2006 IEEE/NLM Life Science Systems and Applications Workshop. Bethesda, MD: IEEE; 2006. p. 1–2. 2761
2762
2763
2764
2765
2766
2767
2768
2769
- [87] Nagy Z, Mukli P, Herman P, Eke A. Decomposing Multifractal Crossovers. Frontiers in Physiology. 2017 Jul;8:533. <https://doi.org/10.3389/fphys.2017.00533>. 2770
2771
2772
2773
2774
2775
2776
2777
2778
2779
2780
2781
2782
2783
2784
2785
2786
2787
2788
2789
2790
2791
2792
2793
2794
2795
2796
2797
2798
2799
2800
2801
2802
2803
2804
2805
2806

```
2807 Appendix
2808
2809 Python code
2810
2811
2812 Sample python code for testing power-law scaling
2813
2814 print("HELLO")
2815
2816
2817
2818
2819
2820
2821
2822
2823
2824
2825
2826
2827
2828
2829
2830
2831
2832
2833
2834
2835
2836
2837
2838
2839
2840
2841
2842
2843
2844
2845
2846
2847
2848
2849
2850
2851
2852
```